Supplementary Material

Unusual irradiation-induced disordering in Cu_3Au near the critical temperature: an *in situ* study using electron diffraction

C.R. Lear,[a] R.S. Averback, and P. Bellon

Department of Materials Science and Engineering, University of Illinois at Urbana-Champaign, Urbana, IL 61801, USA

A.E. Sand

Department of Physics, University of Helsinki - P.O. Box 43, FI-00014 Helsinki, Finland

M.A. Kirk

Nuclear Engineering Division, Argonne National Laboratory, Argonne, IL 60439, USA

I. SUMMARY OF WORK BY LEE[1]

Electrical resistivity measurements across the unirradiated, molecular beam epitaxy grown films of Cu_3Au are presented in Fig. S1a for 100 °C to 450 °C. These data – corrected for purely thermal effects – were converted to equilibrium values of the long-range order parameter S using Muto's relation[2]

$$S^2 = 1 - \frac{\rho_S - \rho_1}{\rho_0 - \rho_1}, \qquad \text{(S1)}$$

Where ρ_S, ρ_0, and ρ_1 are the resistivity of the current film, a disordered film (S = 0), and a fully ordered film (S = 1), respectively. The equilibrium S measured in this way are shown as a function of temperature in Fig. S1b, alongside Cowley's model.[3] Note the increasing underestimation of S with increasing temperature toward the order-disorder transition at T_C = 393 °C.

Measurements of S for the films during 750 keV Ne^+ irradiation are presented in Fig. S2 for select temperatures. Below ~ 300 °C, the films disordered more rapidly with decreasing temperature and did not reach a steady state S. In contrast, the films irradiated at higher temperature reached steady state quickly, with the difference between initial and steady state S increasing with increasing temperature. Closer investigation of this disordering behavior revealed that the initial rate of disordering ε (per displacement per atom) increases with increasing temperature toward T_C, as shown in Fig. 4 of the main text. Further irradiations with 1.0 MeV He^+ irradiation showed that ε is independent of the flux used, Fig. S3a, while the rate with time (i.e., dS/dt) is linear with that flux, Fig. S3b.

II. THINNING AND ION MILLING

Polishing was largely performed using a semiautomatic MultiPrep™ polishing system from Allied High Tech Products and 30 µm to 1 µm diamond lapping films. The finely polished surface was finished by hand on a MetaServ® 250 grinder-polisher from Buehler using a 50 nm alumina suspension on a cloth pad. Once the specimen disks were reduced to 100-150 µm thick, further thinning was performed using a Model 656 Dimple Grinder from Gatan and cubic boron nitride paste. The center thickness of the specimens was first reduced to 30-40 µm using a phosphor bronze wheel, then polished to a thickness of 15-25 µm with felt polishing wheels. The final thinning to

[a] Address correspondence to this author. e-mail: crlear2@illinois.edu, phone: +1 (865) 742-1591

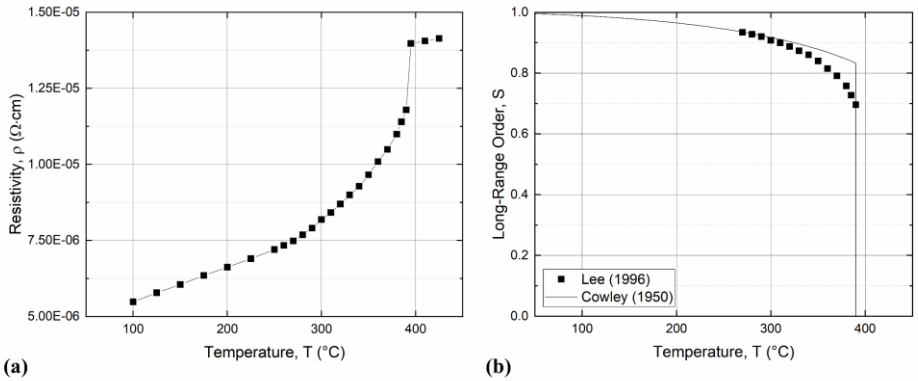

FIG. S1. Measurements of the unirradiated films, adapted from Lee.[1] (a) Resistivity ρ of the films as a function of temperature. (b) Long-range order S of the films as a function of temperature, with Cowley's model[3] for comparison.

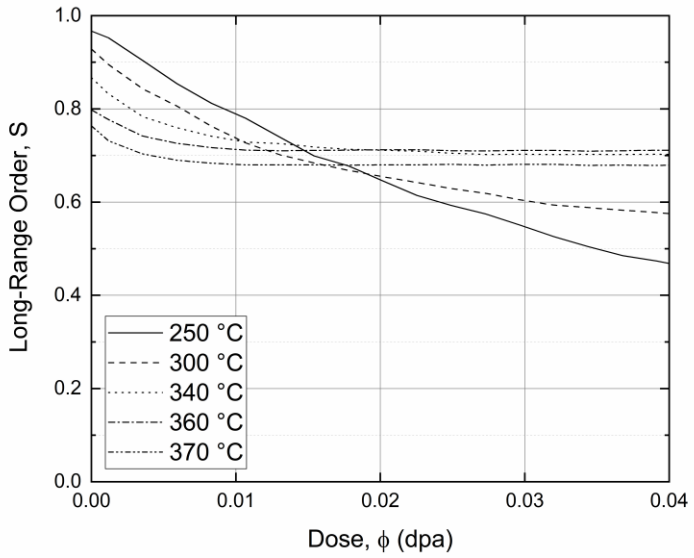

FIG. S2. Evolution of long-range order S with increasing dose ϕ at several irradiation temperatures, adapted from Lee.[1] Irradiation at 250 °C and 300 °C did not lead to a steady state of order within the duration of the experiment, ~ 0.05 dpa, while such states are reached for all higher irradiation temperatures.

electron transparency was carried out using a Model 691 Precision Ion Polishing System (PIPS) from Gatan and simultaneous milling from both dimpled and polished surfaces. Milling proceeded in three stages: (i) to thin the dimpled center to the point of breakthrough (7°/-5°, 5 keV); (ii) to widen or create additional breakthroughs if only a small number of grains would be sampled by the first (5°/-3°, 2.5 keV); and (iii) to remove surface damage from the preceding stages (5°/-3°, 0.5 keV).

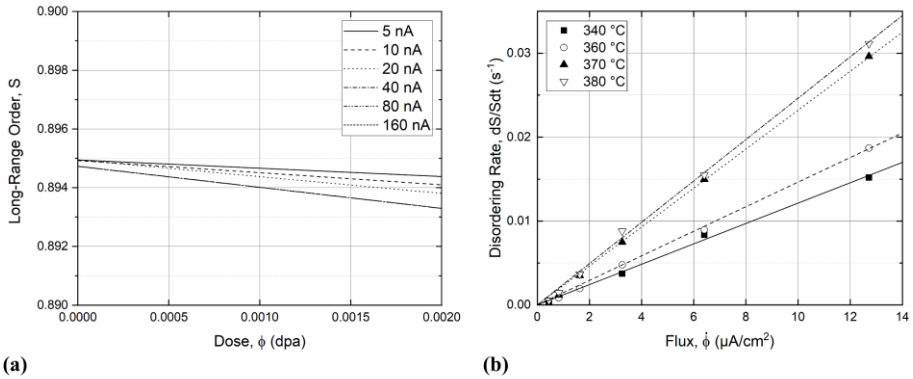

FIG. S3. Initial disordering of Cu_3Au under 1.0 MeV He^+ irradiation, adapted from Lee.[1] (a) Initial evolution of long-range order S with increasing dose ϕ for several irradiation fluxes at 340 °C. (b) Initial disordering rate with time, dS/Sdt, as a function of flux $\dot{\phi}$ for several irradiation temperatures.

III. DIFFRACTION DATA ANALYSIS

Recorded diffractograms and intensity profiles for each irradiation condition were analyzed in series using the *MATLAB* software package.[4] Processing began with the conversion of intensity profiles from images to raw data. Background intensities were then fit and subtracted from the data using the *Backcor* package[5] for *MATLAB*. The area under peaks in the intensity data were integrated individually, and the integrated intensities under the 2*g* and 3*g* peaks were used along with equilibrium values of the same to calculate S using Eq. (4) of the main text. Analysis of each intensity profile was followed by processing of the corresponding diffractogram. Here, we defined regions of interest two lengths of the $\boldsymbol{g}$ vector ("$2|\boldsymbol{g}|$") long and $0.3|\boldsymbol{g}|$ wide, running parallel on each side of and separated from the systematic row of reflections by $0.3|\boldsymbol{g}|$. Pixel values within these regions of interest were binned according to distance along the systematic row, and the center of mass of the resulting distribution was compared with the value from a well-aligned diffractogram. Deviations from this aligned reference were translated into deviations in the Kikuchi band position discussed above. While all such deviations were kept within $\pm 0.25|\boldsymbol{g}|$ for the present results, the impact of large misalignments was investigated separately at room temperature, shown in Fig. S4. This observed relationship between misalignment, in terms of $|\boldsymbol{g}|$, and error in the measurement of S was then used to correct those values obtained from each intensity profile. For each irradiation, the *Origin*[6] and *ImageJ*[7] software packages were used to manually analyze randomly selected intensity profiles and diffractograms, respectively. These tests showed good agreement between automated and manual processing.

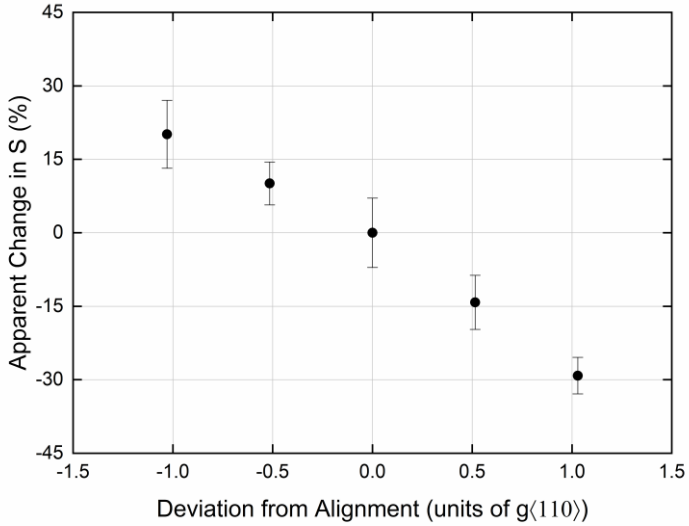

FIG. S4. Change in apparent long-range order *S* (versus true value) with misalignment.

IV. POST-IRRADIATION RECOVERY

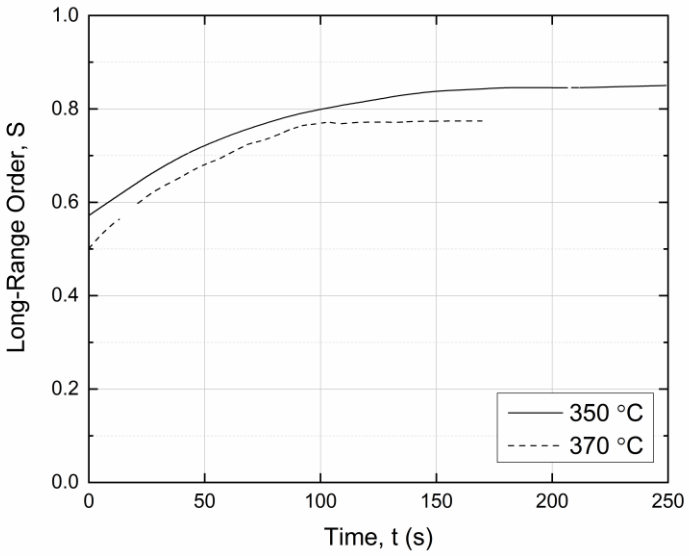

FIG. S5. Recovery of long-range order *S* with time *t* following irradiation.

V. BEAM HEATING EFFECTS

Beam heating effects were estimated using a method adapted from Carslaw[8] for the heating of uniform cylinders with internal heat production. Here, the thickness of our foil specimens is assumed to increase linearly with increasing distance from the center hole, and the change in cross-sectional area must be considered. The principle equation for the steady state temperature thus becomes

$$0 = \frac{d^2(\Delta T)}{dr^2} + \left(\frac{1}{A}\frac{dA}{dr}\right)\frac{d(\Delta T)}{dr} + \frac{Q}{K} = \frac{d^2(\Delta T)}{dr^2} + \frac{2}{r}\frac{d(\Delta T)}{dr} + \frac{Q}{K}, \quad \text{(S2)}$$

where ΔT is the beam heating in Kelvin, r is the radial position, A is the cross-sectional area, Q is the heat production in J/(m^{3}s), and K is the thermal conductivity. The heat production is $Q = \dot{\phi} E_L / b$, where $\dot{\phi}$ is the dose rate in ions/(m^{2}s), E_L is the average energy loss per ion, and b is the foil thickness. Solving Eq. (S2) such that $\Delta T(r = a) = 0$ yields

$$\Delta T(r) = \frac{Q(a^2 - r^2)}{6K}, \quad \text{(S3)}$$

which differs from Carslaw's steady state solution only in the factor of 6 rather than 4. As an example, beam heating across the width of the ion beam according to Eq. (S3) is shown in Fig. S6 for the irradiations at 350 °C and 1.3×10^{16} ions/(m^{2}s) (the highest dose rate used). While the thermal conductivity varies by ~ 30% across the range of temperatures studied here, these slight increases for lower temperature irradiations would not produce appreciable beam heating effects.

VI. MD SIMULATION OF CASCADES

For cascade simulations in Cu3Au, we constructed simulation cells with perfect ordering (i.e., with Au atoms at the corners of a conventional fcc unit cell, and Cu atoms at the cube faces). For the atomic interactions, we used the embedded atom model potentials by Foiles.[9] The Cu-Au interaction is described using an averaging scheme, which has been shown to work well for alloys.[10] At short distances, the potentials were smoothly joined to the ZBL repulsive potential.[11] All simulations were performed with the molecular dynamics code PARCAS.[12] The principles of the molecular dynamics algorithms are presented in Refs. 13 and 14. The adaptive time step is the same as in Ref. 15.

Each cell was first relaxed with Berendsen's temperature and pressure control algorithms,[16] to zero pressure and the desired temperature of 0 K, 470 K, or 660 K. Cascades were initiated from an atom on a lattice site, with initial velocities in random directions and energies between 400 eV and 20 keV. We simulated ten cascades for each temperature and recoil energy. Previous work has indicated that the type of the recoil does not affect results;[17] here, we used Cu atoms as the primary recoils. The temperature at the cell borders was scaled during the simulation, with the Berendsen thermostat, towards the initial ambient temperature, thus mimicking the heat dissipation in the bulk. The cell volume was kept constant during the cascade simulations. Cell borders were monitored for energetic atoms, to ensure that cascades remained within the simulation cell, and thus did not self-interact. Electronic stopping was applied to all atoms with kinetic energies above 10 eV. The simulations were carried out for 30 - 40 ps at 0 K, and for 90 ps at the elevated temperatures. A longer simulation time was necessary at higher temperatures to allow the defect structures in the cascade core region to relax. Interstitial and vacancy defects were identified using the Wigner-Seitz cell method.[13]

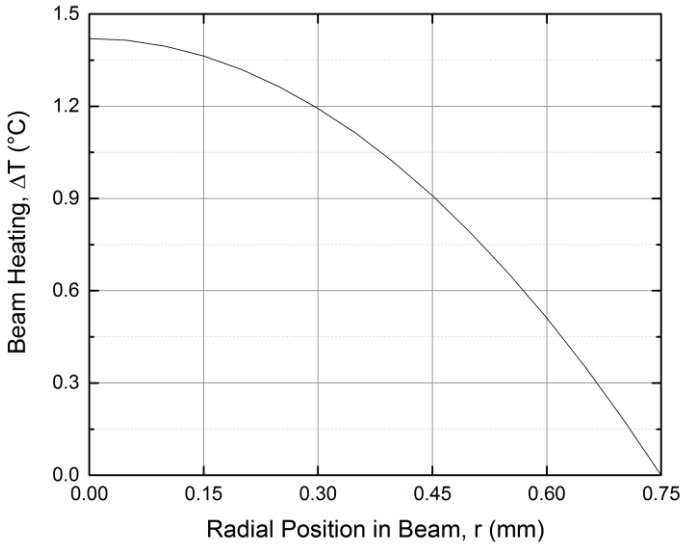

FIG. S6. Estimated beam heating ΔT as a function of radial position *r* in the ion beam.

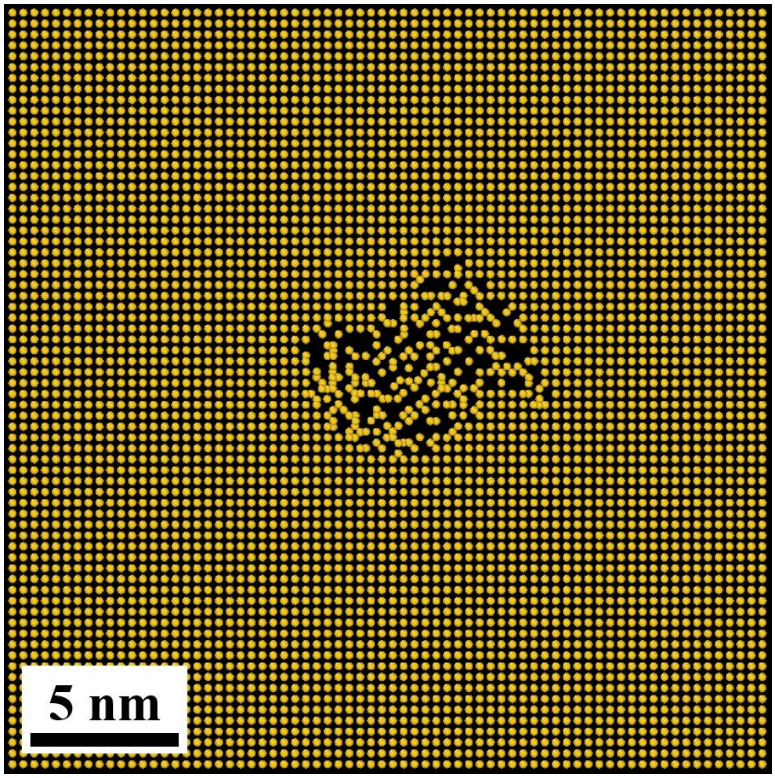

FIG. S7. MD simulation cell of Cu_3Au following cascade damage. For increased visibility, only two (100) planes are shown and all Cu atoms have been removed.

REFERENCES

1. Y. S. Lee: Atomic Transport Mechanisms in Irradiated Cu_3Au. Ph.D. Dissertation, University of Illinois at Urbana-Champaign, Urbana, IL. http://hdl.handle.net/2142/23646 (1996).
2. T. Muto: No Title. *Sci. Pap. Inst. Phys. Chem. Res.* **30** (1936).
3. J. M. Cowley: An Approximate Theory of Order in Alloys. *Phys. Rev.* **77**, 669 (1950).
4. *MATLAB*, version 9.0; numerical programming and computing software; MathWorks, Inc.: Natick, MA (2016).
5. *Backcor*, version 1.4; background fitting and subtraction script for *MATLAB*; V. Mazet (2013).
6. *Origin*, version 2016; scientific graphing and data analysis software; OriginLab Corporation: Northampton, MA (2016).
7. *ImageJ*, version 1.51; image processing software; National Institutes of Health: Bethesda, MD (2016).
8. H. S. Carslaw and J. C. Jaeger: Conduction of Heat in Solids (Clarendon Press, Oxford, 1959).
9. S. M. Foiles, M. I. Baskes, and M. S. Daw: Embedded-atom-method functions for the fcc metals Cu, Ag, Au, Ni, Pd, Pt, and their alloys. *Phys. Rev. B* **33**, 7983 (1986).
10. T. Diaz de la Rubia and A. Caro: Radiation-induced disordering and defect production in Cu_3Au and Ni_3Al studied by molecular dynamics simulation. *Nucl. Instruments Methods Phys. Res. Sect. B Beam Interact. with Mater. Atoms* **81**, 86 (1993).
11. K. Nordlund, L. Wei, Y. Zhong, and R. Averback: Role of electron-phonon coupling on collision cascade development in Ni, Pd, and Pt. *Phys. Rev. B* **57**, R13965 (1998).
12. *PARCAS*; molecular dynamics code; K. Nordlund (2006).
13. K. Nordlund, M. Ghaly, and R. Averback: Defect production in collision cascades in elemental semiconductors and fcc metals. *Phys. Rev. B* **57**, 7556 (1998).
14. M. Ghaly, K. Nordlund, and R. S. Averback: Molecular dynamics investigations of surface damage produced by kiloelectronvolt self-bombardment of solids. *Philos. Mag. A* **79**, 795 (1999).
15. K. Nordlund: Molecular dynamics simulation of ion ranges in the 1 - 100 keV energy range. *Comput. Mater. Sci.* **3**, 448 (1995).
16. H. J. C. Berendsen, J. P. M. Postma, W. F. van Gunsteren, A. DiNola, and J. R. Haak: Molecular dynamics with coupling to an external bath. *J. Chem. Phys.* **81**, 3684 (1984).
17. K. Nordlund, J. Nord, and J. Keinonen: Chemical effects in collision cascades. *Nucl. Instruments Methods Phys. Res. B* **177**, 31 (2001).